13

Optical properties of porous silicon irradiated with a nanosecond ytterbium laser

© N.V. Rybina,[1] N.B. Rybin,[1] V.S. Khilov,[2] V.V. Tregulov,[2] A.I. Ivanov,[2] K.O. Aiyyzhy,[3] N.N. Melnik[4]

[1]Ryazan State Radio Engineering University, Ryazan, Russia
[2]Ryazan State University named for S. Yesenin, Ryazan, Russia
[3]Prokhorov Institute of General Physics, Russian Academy of Sciences, Moscow, Russia
[4]Lebedev Physical Institute, Russian Academy of Sciences, Moscow, Russia
e-mail: nikolay.rybin@yandex.ru

Received December 27, 2024
Revised February 7, 2025
Accepted February 14, 2025

It is shown that by changing the parameters of irradiation with a pulsed nanosecond ytterbium fiber laser, it is possible to influence the information-correlation, fractal and optical properties of the surface of porous silicon films. Using the analysis of the reflection spectra and Raman scattering of light, the relationship between the parameters of laser irradiation of porous films and their optical characteristics is established. The studied semiconductor structures can be relevant for creating antireflective layers of silicon solar cells, as well as chemical sensors.

Keywords: porous silicon, nanosecond laser pulses, morphology, mutual information, fractal analysis, Raman scattering, surface reflectance spectra.

DOI: 10.61011/TP.2025.06.61386.472-24

Introduction

Today, the issue of using porous silicon films (*por*-Si) in fabrication of semiconductor devices has become pivotal. One of the most important properties of *por*-Si is its highly developed surface, which makes it attractive for creating the anti-reflective layers of solar cells, sensitive areas of humidity sensors and chemical gas sensors [1]. From a practical standpoint, it is very important that fabrication of *por*-Si films does not require the use of complex technological equipment and expensive chemical reagents. In order to increase the efficiency of solar cells and flexibly control the functional characteristics of sensors, the task of developing the new technological methods for surface modification is urgent *por*-Si. One of the solutions to this problem is treatment of *por*-Si films with nanosecond laser pulses [2–4]. In [2], it was shown that nanosecond laser pulses 70 ns at a wavelength of 694 nm, in the energy density range of $0.73-1.8\,J/cm^2$ lead to a significant change in the surface morphology of the films *por*-Si, and this effect is a threshold itself. In paper [3] it was demonstrated that laser irradiation with a pulse of 80−100 ns in the energy density range of $5-7\,J/cm^2$ leads to oxidation of *por*-Si, resulting in formation of $Si:SiO_2$ in the near-surface layer. The study [4] was focused on the effect of a pulsed ytterbium optical fiber laser with a wavelength of 1064 nm, pulse duration 4−30 ns and power 4−12 W on the surface of *por*-Si. The research proved that irradiation modes affect the information and correlation characteristics of hbox*por*-Si surface. Pulsed laser irradiation of *por*-Si films allows formation of silicon nanoparticles used in biophotonics [5].

Irradiation of *por*-Si film, pre-doped with boron, with laser pulses with a wavelength of 1064 nm and a duration of 200 ns, forms a layer of amorphous silicon with a Fano resonance on its surface [6]. Metasurfaces of amorphous silicon with Fano resonance are relevant for problems of nonlinear holographic visualization, laser beam control, and generation of entangled photons by spontaneous parametric transformation with frequency reduction [7]. Therefore, the study of the effect of pulsed laser radiation on physical properties of *por*-Si films remains urgent.

The purpose of this work is to study the effect of nanosecond laser pulse irradiation of hbox*por*-Si films pre-grown on silicon single crystal substrates by metal-stimulated etching on their morphology and optical properties.

1. Samples fabrication technology

For fabrication of the studied samples, silicon single-crystal wafers of *p*-type of conductivity, with a resistivity of $1\,\Omega\cdot cm$ and a surface orientation (100) were used. *por*-Si films were grown by method of a two-stage metal-stimulated etching.

During the first stage the silicon wafer surface was sputtered with the silver particles from the solution: Ag_2SO_4 (0.01 M), HF (46 %), C_2H_5OH (92 %) at a ratio of components 1:0.1:0.3 during 20 s. The wafer then was washed in distilled water.

At the second stage, the wafer with the sputtered silver particles was immersed in the solution: H_2O_2 (1.24 M), HF (46 %), C_2H_5OH (92 %) at the ratio of components 1:0.5:0.25 and was hold during 60 min. Porous structure was formed as a result. Further, the samples were washed in the

distilled water, and then in concentrated HNO_3 for 60 min to remove silver particles from pores. Finally, the samples were washed by distilled water to remove traces of reagents and reaction products, and dried in drying cabinet.

It is important to note that the structural properties of *por*-Si films largely depend on the method of their growth [8]. In this paper, we study *por*-Si films formed by metal-stimulated etching. Such films are usually classified as an ensemble of silicon nanowires [9,10].

The films *por*-Si were irradiated with a pulsed ytterbium fiber laserYLPM-1-4x200-20-20 (IPG Photonics, Russia) with a wavelength of 1064 nm. The laser beam scanned the surface of *por*-Si film at a speed of 150 mm/s and a pulse repetition rate of 20 kHz. The treated area of *por*-Si film was 10×10 mm. The surface was irradiated with (τ) 4–30 ns pulses with an average power of (P) 0.2–5.6 W.

It should be noted that for the laser used, the average power value depends on the pulse duration. When irradiated the wafer with *por*-Si film was located in a cuvette filled with isopropanol. The isopropanol layer thickness above the sample surface was 5 mm. Use of isopropanol is caused by minimization of intensity of oxidation of silicon crystallites of *por*Si film. Irradiation modes of samples P and τ, are listed in the table.

2. Method of study of experimental samples

Images of the frontal surfaces of hbox*por*-Si experimental samples were obtained using a scanning electron microscope JSM-6610LV (JEOL, Japan). The morphology of the samples was studied in the secondary electron imaging (SEI) mode with an accelerating voltage of 30 kV. In order to clarify the morphology of *por*-Si, the obtained images were analyzed using the average mutual information method and the fractal analysis method.

Method of Average Mutual Information (AMI [11,12]) based on information theory and ensures determination of imperfections, distortions of the surface relief. The quantitative indicator of AMI characterizes the degree of order. The indicator of maximal mutual information (MMI) characterizes the information capacity of the surface.

The term „fractal“ was formulated by B.Mandelbrot and describes a set with a fractional dimension [13]. The main parameter for describing the morphology of fractal surfaces is the fractal dimension (D), which is the degree of scalability of the set of elements that make up the complete image of the surface [13]. Fractal analysis of the sample surface was performed using ImageJ program with FracLac library [14].

In order to clarify the features of the microstructure of *por*-Si films, the Raman scattering (RS) spectroscopy method was used. RS spectra were measured by spectrometer in-Via (Renishaw, Great Britain). RS excitation was carried out by a solid-state laser at a wavelength of 785 nm, the radiation power was 0.22 mW, the accumulation time was — 20s, the number of accumulations — 2, the magnification of the lens was 50x. When measuring the RAMAN spectra, there was no effect of laser-induced heating of the sample. RS excitation and detection took place in a standard geometry, when the laser beam and scattered light are directed along the normal to the frontal surface of the sample film. RS spectra were measured in a micro-probe mode in „back scattering“ geometry.

To characterize the optical properties of *por*-Si films the diffuse reflectance spectra with the wavelengths of 300–1100 nm were studied by means of spectrophotometer SF-56 (LOMO, Russia).

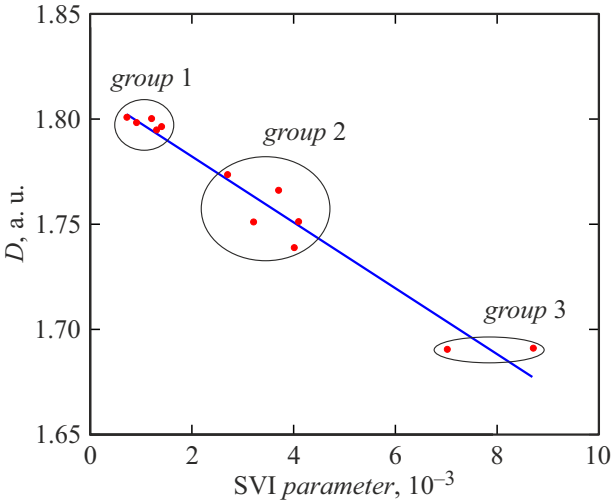

Figure 1. Fractality dimension D versus AMI index.

3. Research results

Physical quantities characterizing the irradiation modes, morphological features, and the results of the study of Raman scattering spectra of experimental samples are given in the table.

From the table we see that with the growth of P at fixed value of τ the AMI index rises. At the same time, there is a tendency to decrease the fractality index D. The increase in AMI index is explained by an increase in the degree of ordering of the structural elements of the surface [11,12]. Lower D indicates an increase in correlations in the silicon crystallite system [13,14]. There is no correlation between the values of MMI and P at a fixed value of τ (see table). The value of MMI index for all samples lies in the range 0.5–0.7, which indicates that the surface of the samples has an average information capacity [11,12].

Fig. 1 shows the fractality index D dependence on AMI parameter. Here we may distinguish three separate areas, which are highlighted by solid contours (Fig. 1). In view of this circumstance, the studied samples may be divided into 3 groups (Fig.1, see the table).

Physical quantities characterizing the irradiation modes, morphological features, and the results of the study of RAMAN spectra of experimental samples

Sample №	Irradiation		Morphology				RS	
	P, W	τ, ns	AMI $\cdot 10^{-3}$	MMI	D	№ of group	d, nm	σ,MPa
1	–	–	0.7	0.511	1.80	1	32	–
2	0.2	4	0.9	0.544	1.80	1	32	–
3	0.4	4	3.0	0.630	1.75	2	28	–
4	0.7	4	3.2	0.604	1.75	2	12.4	–
5	0.9	4	4.0	0.595	1.74	2	12.4	–
6	0.6	8	1.4	0.651	1.80	1	32	–
7	1.2	8	4.1	0.602	1.75	2	28	–
8	2.4	8	4.6	0.633	1.74	2	28	–
9	1.1	20	1.2	0.624	1.80	1	38	–
10	2.2	20	1.3	0.578	1.80	1	38	–
11	3.4	20	3.7	0.581	1.77	2	36	–
12	1.4	30	2.	0.562	1.77	2	36	–
13	2.4	30	7.0	0.527	1.69	3	–	10.5
14	5.6	30	8.7	0.621	1.69	3	–	26.4

Fig. 2 illustrates SEM images of the surface of *por*-Si film for typical samples of 1–3 groups. We see that morphology of surface of samples in various groups differs greatly. When *por*-Si film is irradiated with a laser, intensive removal of particles from the surface is observed (under all irradiation modes). Due to the removal of particles, the thickness of *por*-Si film decreases, as can be seen in the insert windows of SEM images. By using SEM method to study *por*-Si film of the irradiated samples it was demonstrated that the surface of silicon crystallites is rounded. This is generally observed during melting. Deep in *por*-Si film the crystallites were not melted. The surface of the samples of group №1 (Fig. 2, *b*) is homogeneous with the presence of similar particles of the order 2,μm in diameter. The surface of the №2 group samples has a more developed relief, with a fractal-like structure, and relief depressions are clearly visible (Fig. 2, *c*). The surface of the №3 group samples (Fig. 2, *d*) is no longer a fractal-like structure, but a smoother one, with the presence of large (5–8,μm in diameter) spherical particles on it. Probably, for the 3rd group of samples, a stronger effect of laser radiation (both in pulse duration and radiation power) led to the occurrence of melting processes and the formation of large particles from the liquid phase. Thus, an increase in the pulse duration from 4 to 30 ns and the average pulse power of laser radiation from 0.2 to 5.6 W leads to a significant transformation of the surface morphology of *por*-Si films.

In order to study the structural features of *por*-Si films, the Raman scattering spectra of experimental samples were studied at the nanoscale level. Figure 3 shows RS spectra of the initial silicon substrate (curve *1*), sample №1 (curve *2*), which was not irradiated with laser, samples №2 and №3 (curve *3*), samples №4–№14 (curve *4*). RS spectra of samples №4–№14 practically coincide.

The spectral line 521 cm^{-1} characterizes the fundamental oscillation of the silicon crystal lattice (Fig. 3) [15]. The line 302 cm^{-1} is caused by a transverse acoustic phonon of the second order 2TA and is peculiar to the monocrystalline silicon [16]. The presence of this line on RS spectra of all the studied samples with the *por*-Si film, as well as the substrate, indicates that when growing *por*-Si film, as well as after its laser irradiation, the silicon lattice has not undergone any serious disruptions (Fig. 3). The wide band in the range of 930–1000 cm^{-1} is due to silicon RS second-order line [15].

In RS spectra of samples №2–№14 (curves *3* and *4* in Fig. 3) the lines 135 and 480 cm^{-1}, peculiar to amorphous silicon can be observed [17,18]. However, the intensity of these lines is much lower compared to 302 cm^{-1} line. This also indicates that laser irradiation of *por*-Si film of samples №2–№14 does not lead to significant disturbances in the silicon lattice, amorphization is negligibly small.

RS spectral line 610 cm^{-1} is observed due to an electrically-active boron impurity in the silicon [19]. For

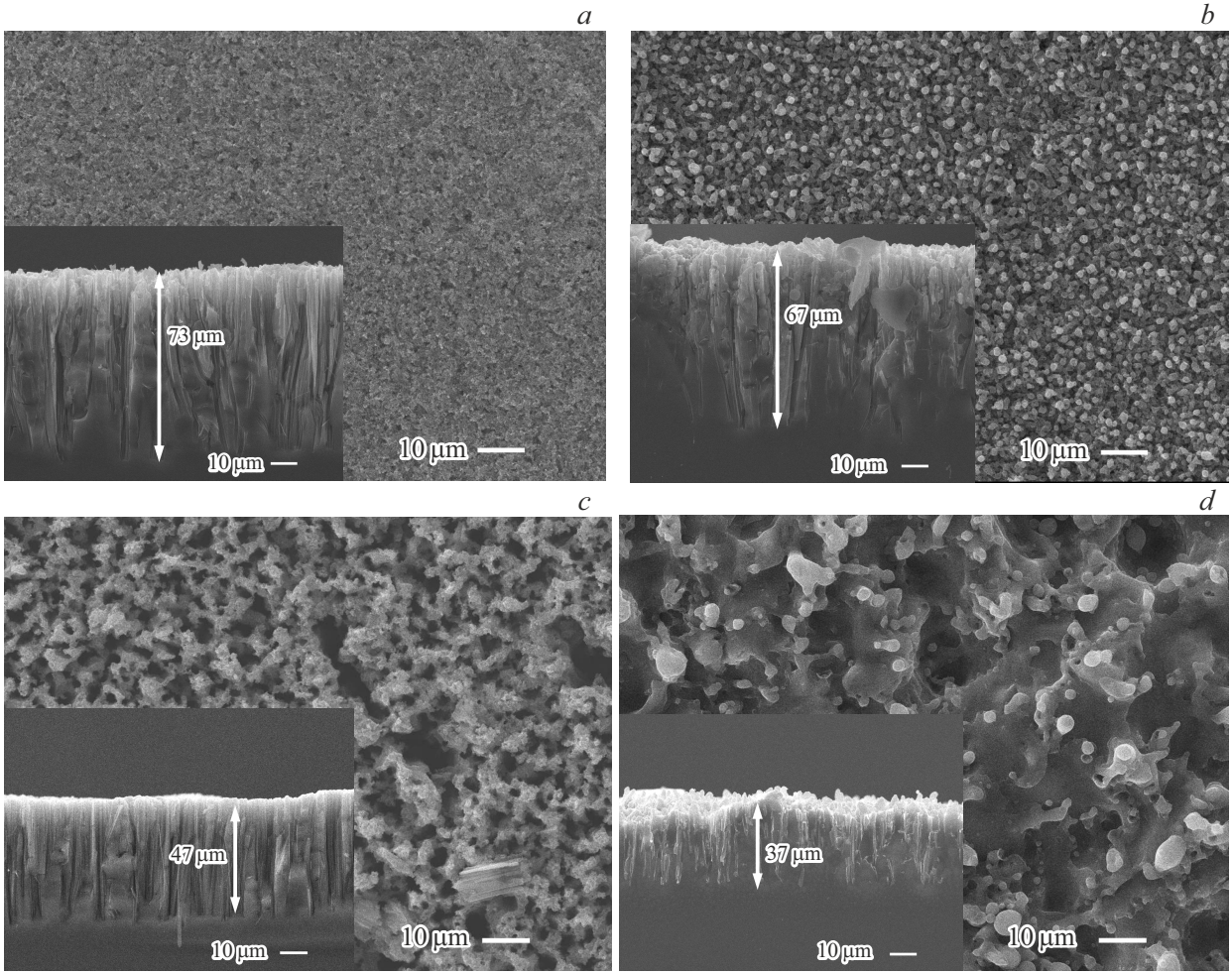

Figure 2. Samples surface images obtained by a scanning-electron microscope: *a* — sample№1 without irradiation by laser, *b* — sample №2 of group 1, *c* — sample №3 of group 2, *d* — sample №13 of group 3. The tabs show the structures of the samples in the section with the average thickness of the porous layer.

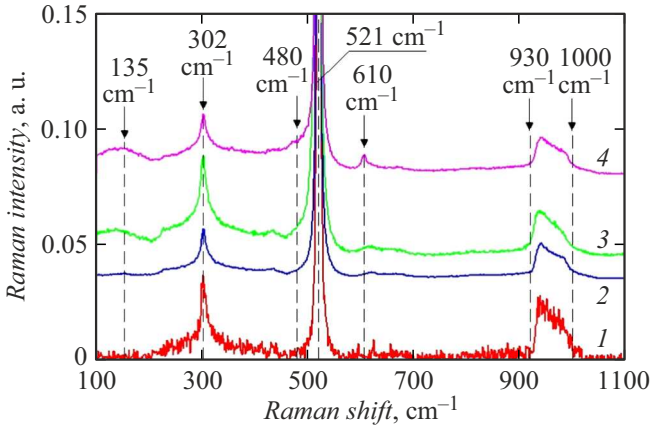

Figure 3. RS spectra: single crystal silicon substrate (*1*), as well as samples № 1 (*2*); № 2 and № 3 (*3*); № 4–№ 14 (*4*).

samples №2–№14 (curves *3* and *4* in Fig. 3), an increase in the intensity of this line is observed compared with the substrate (curve *1* in Fig. 3) and sample №1 (curve *2* in Fig. 3). This may be due to the redistribution of an electrically active boron impurity during recrystallization of silicon crystallites of hbox*por*-Si film caused by laser irradiation of samples №2–.

Figure 4 shows RS spectral line of the fundamental oscillation of a silicon lattice near frequency 521 cm^{-1} for a single-crystal substrate, as well as of samples No1–№14. For the samples №9–№12 spectral lines 521 cm^{-1} are practically merging and located between the curves designated by „•“ and „○“.

For samples №1–№12, the spectral line under consideration is noticeably shifted towards low frequencies and has a broadening compared to this line of a single-crystal substrate. According to [20], this is explained by the effect of the spatial limitation of phonons in ensembles of nanoscale silicon crystallites of *por*-Si film. According to the method presented in [20], the average diameter of

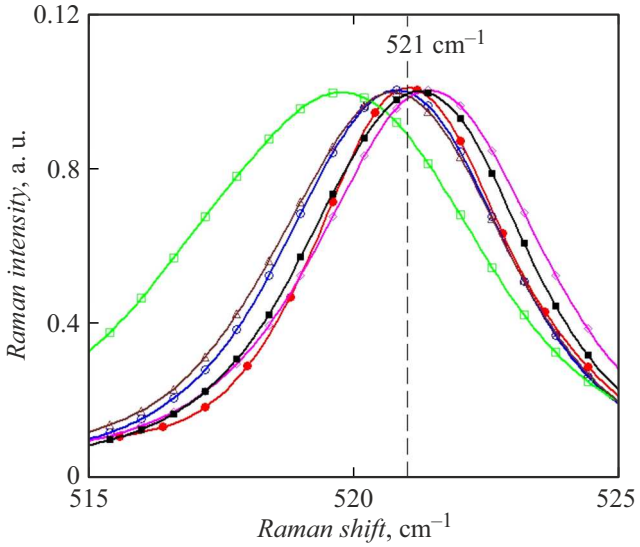

Figure 4. RS spectra of the fundamental oscillation line of a silicon lattice near frequency 521 cm^{-1} for a single-crystal silicon substrate (●), as well as samples №1, №2, №6 (○); №4, №5 (□); №3, №7, №8 (Δ); №13 (■); №14 (◊).

silicon crystallites $d$in *por*-Si film of samples №1–№12 was determined. The values of d are given in the Table.

Thus, we may say that *por*-Si films of samples №1–№12 are formed by the ensembles of silicon nanowires.

For samples №13 and №14, the positions of the maxima of RS spectral lines of silicon lattice fundamental oscillation are shifted towards high frequencies relative to this line of the monocrystalline substrate. This may indicate the occurrence of tensile mechanical stresses [21] as a result of laser irradiation of *por*-Si film. The amount of mechanical stress σ in *por*-Si film can be estimated using the formula

$$\sigma = -52.7\Delta\omega,$$

where $\Delta\omega = \omega - \omega_0$, ω_0 and ω are positions of the maxima of the first-order RS spectral line of silicon in the absence and presence of mechanical stresses, respectively, the value of σ is expressed in MPa [21]. The value ω_0 is 521.0 cm^{-1}, for sample №13ω = 521.2 cm^{-1}, for sample №14 ω = 521.5 cm^{-1}, the values σ are shown in the table.

Analyzing the behavior of the spectral line of the silicon lattice fundamental oscillation near frequency 521 see^{-1} for samples №1–№14, the following patterns may be noted. The largest spread of values d (12.4–36 nm) is observed for the group 2 of test samples (see table). The group 2 includes the samples with the lowest values d (see Table). For group 1 the value d changes not so intensely (32–38 nm). For samples of group 3, there is no effect of phonon spatial restriction, at the same time, tensile mechanical stresses occur here.

The diffuse reflectance spectra of the studied samples, grouped according to the table, are shown in Fig. 5.

It is important to note that the reflection spectra of the samples within each group are close to each other. In connection with this circumstance, the spectra of samples for group №2 („■“ in Fig. 5) and №10 („□“ in Fig. 5) are presented, the spectra of the remaining samples of this group are located between the indicated curves and are not shown in Fig. 5. The exception in this group is sample No1, which was not exposed to laser radiation („Δ“ in Fig. 5), however, in terms of the growth rate of the reflectance coefficient in the wavelength range 500–1100 nm, it is close to the samples of group 1. For group 2 the reflectance spectra for samples №4 („●“ in Fig. 5) and №12 (symbol „○“) are given. The spectra of the remaining samples of this group are located in the region bounded by the spectra of samples №4 and №12. Group 3 contains only two samples — №13 and №14 — they are represented by the symbols „◊“ and „♦“ in Fig. 5, respectively.

On the reflection spectra of the studied samples (Fig. 5), two markedly different regions can be distinguished: the short-wave region, where the reflectance coefficient decreases, and the long-wave region, where this coefficient rises.

The short-wavelength region for samples of groups 1–3 is in the wavelength range of 300–480 nm (Fig. 5). For sample №1, which was not irradiated with a laser, this region is poorly expressed and is in the range of 300–340 nm (Fig. 5). Lower reflectance coefficient in the short-wavelength region may be explained by the absorption of light in silicon nanoscale crystallites [22], which is confirmed by analyzing the Raman spectra (see table). Moreover, the samples №4 and №5 (Fig. 5) belonging to the hbox2nd group have the lowest reflectance, for them the lowest average size of silicon crystallites is 12.4 nm (see table). For samples of group 3 in the short-wave region, the reflectance coefficient is significantly higher compared to the rest of the samples. This can be explained by the absence of the effect of phonon spatial restriction (see table) in the *por*-Si film formed by large crystallites.

The long-wave region includes the visible and near-infrared regions of the spectrum, in the range of 480–1100 nm. Here, for samples of groups 1 and 2, the reflectance coefficient increases more noticeably compared

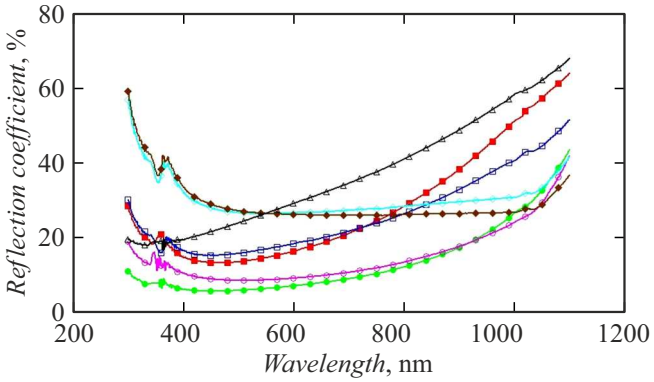

Figure 5. Diffuse reflectance spectra of samples in groups 1 (■, □, Δ), 2 (●, ○), 3 (♦, ◊).

to samples of group 3. According to [22,23], a change in the reflectance coefficient in the specified spectral region may be due to light scattering in silicon crystallites with dimensions of 100−500 nm, which leads to increased scattering of Mie. As a result the reflectance coefficient rises [22]. Thus, a rather intense increase in the reflectance coefficient in the long-wave region for samples of groups 1 and 2 (Fig. 5) may be due to a significant variation in the sizes of silicon crystallites of submicron sizes. Lower growth rate of the reflectance coefficient for group 3 samples in the range of 480−1000 nm (Fig. 5) may be due to a decrease in the size spread of submicron silicon crystallites under the influence of laser irradiation of *por*-Si film.

It should be noted that a decrease in the thickness of *por*-Si films grown by metal-stimulated etching leads to a lower reflectance coefficient of the surface [22]. At the same time, the analysis of the reflectance spectra in Fig. 5 shows that there is no correlation between the thickness of *por*-Si films (Fig. 2) and the reflectance coefficient. In this regard, the nature of the reflectance spectra in Fig. 5 is mainly found from the absorption of light in near-surface silicon crystallites of different sizes.

4. Findings of the study

With the growth of P at a fixed value of τ, there is a rise in AMI index and a decline in fractal dimension D (see table). This may indicate an increase in the degree of ordering of the surface structural elements and a rise of correlations of the silicon crystallites structure [11–14] in submicron and micron scales. The surface of all samples is characterized by an average information capacity, as MMI index varies in the range of 0.5−0.7 [11,12].

The analysis of fractal dimension D versus AMI index (Fig. 1) allows us to classify the studied samples in three groups with different morphological patterns, which can be visually traced in Fig. 2. The surface relief of the samples from groups №1 - №3 becomes more developed and has a more sophisticated structure.

For samples №3−№5, as well as №7−№12 laser irradiation results in the change of average dimension of silicon crystallites d (see the table). The lowest values d are observed for samples №4 and №5 (see the table). As noted in jcite24, at $\tau \sim 1$ ns or less, nanoscale structures are formed on the laser-irradiated surface. Due to small dimensions of nanostructures, the surface tension of the melt of the irradiated surface tends to smooth them out, therefore, a short pulse duration and an energy density close to the melting threshold of the surface material are necessary to form stable nanostructures. [24,25]. Perhaps this explains the minimum values d of samples №4 and №5. For sample №2 there's no any observed changes of d compared to the non-irradiated sample №1, and for sample №3 d declines insignificantly. Apparently, for samples №2 and №3, the melting threshold of the silicon crystallite surface is not reached, therefore, a significant decrease in d is not observed here (see table). For samples №6−№12, the value of d varies slightly, which may be due to the large values of τ.

The *por*-Si film of samples №13 and №14 contains tensile mechanical stresses (see table), which may result from the recrystallization of *por*-Si under the action of laser irradiation. Also, melting and subsequent recrystallization of *por*-Si film under laser irradiation can lead to a redistribution of boron impurities, as evidenced by the transformation of RS spectral line near 610 cm^{-1} in Fig. 3.

Irradiation of *por*-Si film with nanosecond laser pulses significantly changes the nature of reflectance spectrum of its frontal surface (Fig. 5). As shown in [26], small- and large-scale formations emerge on the surface as a result of exposure to laser radiation, and the distribution of their average sizes depends on the irradiation parameters. The morphology of the surface largely determines its optical properties. In the short-wave region (300−480 nm), the nature of the reflectance spectra of the studied samples (Fig. 5) is determined by the absorption of light in nanoscale silicon crystallites. Moreover, the lowest reflectance coefficient is observed for samples with the lowest values of d. In the long-wave region of the spectrum (480−1100 nm), which includes visible and near-infrared regions, the reflection mechanism is determined by scattering of Mie in silicon crystallites with dimensions of 100−500 nm.

The diffuse reflectance spectra of the surface of samples of groups 1−3 (see table) differ markedly (Fig. 5). The samples of group 2 have the lowest reflectance coefficient in the entire studied spectral range (Fig. 5), which may be relevant for the formation of anti-reflective layers of silicon solar cells.

Conclusion

The research proved that by changing the irradiation parameters with a pulsed nanosecond ytterbium fiber laser, it is possible to impact the information-correlation, fractal, and optical properties of the surface of porous silicon films. Based on the results obtained by fractal analysis and average mutual information, the samples were divided into groups with similar properties. By analyzing the RS spectra and reflectance for each group of samples the average sizes of crystallites of irradiated *por*-Si films were obtained. The results obtained can be used to create anti-reflective layers of silicon solar cells, as well as chemical sensors.

The study was carried out using the equipment of the Regional Center for Probe Microscopy for Collective Use at the V.F. Utkin Ryazan State Radio-technical University (RGRTU).

Conflict of interest

The authors declare that they have no conflict of interest.

References

[1] *Handbook of porous silicon. Edited by Leigh Canham* (Springer International Publishing AG, part of Springer Nature, 2018), 1578 p. DOI: 10.1007/978-3-319-71381-6

[2] M.S. Rusetsky, N.M. Kazyuchits, G.D. Ivlev. Sb. nauch. tr. III Mezhdunar. nauch. konf. (Minsk, Republic of Belarus, 2008), p. 150.

[3] L.M. Sorokin, V.I. Sokolov, A.P. Burtsev, A.E. Kalmykov, L.V. Grigor'ev. Pis'ma v ZhTF, **33** (24), 69 (2007). (in Russian)

[4] N.V. Rybina, N.B. Rybin, V.S. Khilov, V.V. Tregulov, Yu.N. Gorbunova. ZhTF, **94** (5), 817 (2024) (in Russian). DOI: 10.61011/JTF.2024.05.57821.24-24

[5] S.V. Zabotnov, D.A. Kurakina, F.V. Kashaev, A.V. Skobelkina, A.V. Kolchin, T.P. Kaminskaya, A.V. Khilov, P.D. Agrba, E.A. Sergeeva, P.K. Kashkarov, M.Yu. Kirillin, L.A. Golovan'. Kvant. elektron., **50** (1), 69 (2020) (in Russian). DOI: 10.1070/QEL17208

[6] N.N. Melnik, V.V. Tregulov, V.S. Khilov, N.V. Rybina, N.B. Rybin, D.S. Kostsov. Kr. soobsch. po fisike FIAN, **11**, 52 (2024) (in Russian). DOI: 10.3103/S1068335624600785

[7] D. Hahnel, C. Golla, M. Albert, Th. Zentgraf, V. Myroshnychenko, J. Förstner, C. Meier. Light Sci. Appl., **12**, 97 (2023). DOI: 10.1038/s41377-023-01134-1

[8] G. Korotchenkov. *Porous Silicon: From Formation to Application* (London: CRC Press, 2016), ISBN: 9780367575328

[9] H. Han, Zh. Huang, W. Lee. Nano Today, **9** (3), 271 (2014). DOI: 10.1016/j.nantod.2014.04.013

[10] A. Efimova, A. Eliseev, V. Georgobiani, M. Kholodov, A. Kolchin, D. Presnov, N. Tkachenko, S. Zabotnov, L. Golovan, P. Kashkarov. Opt. Quant. Electron., **48** (4), 232 (2016). DOI: 10.1007/s11082-016-0495-0

[11] A.V. Alpatov, S.P. Vikhrov, N.V. Vishnyakov, S.M. Mursalov, N.B. Rybin, N.V. Rybina. FTP, **50** (1), 23 (2016). (in Russian)

[12] S.P. Vikhrov, T.G. Avacheva, N.V. Bodyagin, N.V. Grishankina, A.P. Avachev. FTP, **46** (4), 433 (2012) (in Russian).

[13] B.M. Smirnov *Fizika fraktal'nykh klasterov* (Nauka, M., Ed.in chief Fizmatlit, M., 1991), p. 136. (in Russian)

[14] A. Karperien. *FracLac Advanced User's Manual* (Charles Sturt University, Australia, 2005), 36 p. URL: https://www.researchgate.net/publication/238733659 (accessed: 25.04.2024).

[15] W.J. Salcedo, F.R. Fernandez, J.C. Rubimc. Brazilian J. Phys., **29** (4), 751 (1999).

[16] V. Lavrentiev, J. Vacik, V. Vorlicek, V. Vosecek. Phys. Status Solidi B, **247** (8), 2022 (2010). DOI: 10.1002/pssb.200983932

[17] A.T. Voutsas, M.K. Hatalis, J. Boyce, A. Chiang. J. Appl. Phys. **78**, 6999 (1995). DOI: 10.1063/1.360468

[18] K. Shrestha, V.C. Lopes, A.J. Syllaios, C.L. Littler. J. Non Cryst. Solids, **403** (1), 80 (2014). DOI: 10.1016/j.jnoncrysol.2014.07.013

[19] F. Cerdeira, T.A. Fjeldly, M. Cardona. Phys. Rev. B, **9** (10), 4344 (1974).

[20] M. Yang, D. Huang, P. Hao. J. Appl. Phys., **75** (1), 651 (1994).

[21] Qiu Li, Wei Qiu, Haoyun Tan, Jiangang Guo, Yilan Kang. Opt. Lasers Eng., **48** (11), 1119 (2010).

[22] G.K. Musabek, D. Ermukhamed, Z.A. Suleimenova, R.B. Asilbayeva, V.A. Sivakov, I.N. Zavestovskaya, V.Yu. Timoshenko. Kr. soobsch. po fisike FIAN, 10, 23 (2019) (in Russian).

[23] Sh. Kato, Y. Kurokawa, Y. Watanabe, Y. Yamada, A. Yamada, Y. Ohta, Y. Niwa, M. Hirota. Nanosc. Res. Lett., **8**, 216 (2013). DOI: 10.1186/1556-276X-8-216

[24] E.V. Barmina, E. Stratakis, K. Fotakis, G.A. Shafeev, Kvant. elektr., **40** (11), 1012 (2010) (in Russian).

[25] J. Bonse, S. Hohm, S.V. Kirner, A. Rosenfeld. J. Kruger. IEEE J. Selected Topics Quant. Electron., **23** (3), 9000615 (2017).

[26] S.A. Akhmanov, V.I. Yemelyanov, N.I. Koroteev, V.N. Seminogov. UFN, **147** (4), 675 (1985) (in Russian).

Translated by T.Zorina